

Experimental Methods for Determining Residual Stresses and Strains in Various Biological Structures

D. Nelson

Received: 1 July 2013 / Accepted: 4 September 2013 / Published online: 19 November 2013
© Society for Experimental Mechanics 2013

Abstract Over the years, an assortment of methods for determining residual stresses has been developed in the field of experimental mechanics. Adaptations of those methods to study residual strains and stresses in various biological structures found in humans, other mammals, viruses and an insect are reviewed. Methods considered include deflections from release of residual stresses, hole drilling and ring coring, strains upon dissection, the contour method, slitting (crack compliance), X-ray diffraction, photoelasticity, and membrane and shell displacements. Sources of residual stresses and strains are summarized and examples of their physiological role noted.

Keywords Residual stress · Biological · Measurement methods · Tissue · Prestress

Introduction

Experimental methods for determining residual stresses have been developed largely for engineering materials. In recent years, the existence, formation and role of residual stresses in biological structures have been studied by biomechanical researchers. The purpose of this paper is to provide an overview of how methods used for engineering materials have been extended to study residual stresses in various biological structures. It is hoped that this overview will be of interest to researchers in experimental mechanics and potentially encourage development of new or improved methods for determining residual stresses in structures ranging from arteries to viruses. To keep the scope of the paper reasonable, the

overview will be limited to naturally occurring residual stresses (as opposed to those that may develop as result of medical implants or dental procedures). As with engineering components, residual stresses in biological structures are taken to mean those that exist in the absence of applied forces. Residual *strains* in biological structures can be especially important too, as will be shown subsequently. Although the focus of this paper is on experimental methods for determining residual stresses and strains (RSS), mechanisms that induce RSS in tissues will be summarized as background, along with examples of the significance of RSS.

Growth, remodeling and morphogenesis can generate RSS [1–13]. Remodeling can have different meanings, but will refer here to a change in structure or properties, often in response to a physiological change such as the onset of high blood pressure. Morphogenesis refers to the formation or shaping of an organism or biological structure. As an example of a mechanism that generates RSS, suppose that individual elements of tissue could grow without constraint from adjacent tissue, each producing “growth strain” [4]. When such isolated elements are brought back together to form a continuous body, the growth strains are often incompatible, generating a residual stress field. A similar mechanism exists in engineering materials and is common in trees [14]. Models of growth based on mixture theory [15–17] also predict the formation of RSS. Non-uniform osmotic swelling of tissue may contribute to the development of RSS as well [18, 19]. Stress and strain modulate growth, remodeling and morphogenesis [1–4, 20–24], and thus an interplay can exist between RSS and those processes. For instance, RSS are believed to influence bone healing [25] and morphogenesis of a developing heart [26] and limbs [27].

In arteries, compressive circumferential RSS are important because they counteract stresses from blood pressure [28–31], and as a result, may increase resistance to failure [32] (e.g., aortic tearing) and reduce the risk of rupture of atherosclerotic

D. Nelson (✉)
Mechanical Engineering Department, Stanford University, Stanford,
CA 94305-4021, USA
e-mail: dnelson@stanford.edu

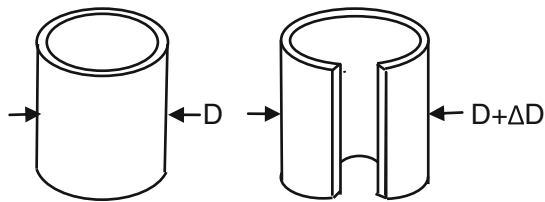


Fig. 1 Change in diameter after slitting to release circumferential residual stress

plaque [33], an event that leads to clots. RSS in arteries increase with the development of high blood pressure [34, 35], serving to reduce stresses on tissue at the inner diameter. Longitudinal RSS enable arteries to sustain blood pressure pulses with minimal variation in length [36]. In addition to such physiological roles, RSS are of clinical significance. For example, a longitudinal incision in an artery will cause newly created surfaces to spring open. RSS governs the size and shape of openings and are important in computational simulations of coronary bypass surgery [37] and angioplasty [38]. Similarly, the size and shape of surgical incisions in skin depends on RSS, which also influence scar formation [39] and the suturing forces needed to close wounds [40].

Deflections Upon Release of Residual Stresses

Opening Angle Method

A long standing approach for finding residual hoop stresses in thin-walled tubing involves slitting a length of tube longitudinally, causing it to spring open upon release of residual stresses, as in Fig. 1. The bending moment released can be estimated from a relation involving cross sectional moment of inertia, modulus of elasticity, Poisson's ratio and change in diameter [41]. The portion of hoop residual stresses associated with bending through the wall can then be computed.

A similar experimental approach has been adopted in the biomechanics of arteries, but with constitutive relations appropriate for biological tissue. In the 1980s, Fung [42] and Vaishnav and Vossoughi [43] found that when a length of an artery was dissected to produce a ring and then slit radially through the wall, it became a sector like that depicted in idealized form in Fig. 2. Chuong & Fung [44] obtained an analytical solution for circumferential residual strains based on measurement of “effective”

Fig. 2 Deflection of an arterial ring after slitting

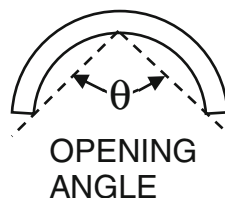
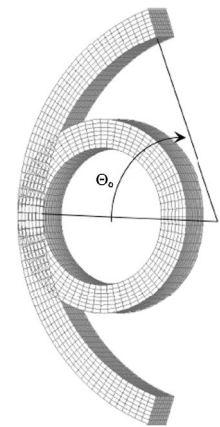


Fig. 3 Schematic of arterial ring in opened and original configurations [45]



values of opening angle and associated radii that accounts approximately for the non-circular cross-sections of actual arteries. They analyzed the effect of residual strains on stresses from blood pressure by considering the bending deformation needed to restore the opened ring to a circular shape, using a homogeneous, cylindrically orthotropic, nonlinear elastic, incompressible material model to describe arterial tissue. They were pioneers in recognizing the significance of RSS in arteries and their work has led to numerous studies by other researchers.

Figure 3 shows a finite element model that illustrates conceptually how residual stresses may be computed by restoring an opened arterial ring to its original configuration. It turns out that magnitudes of compressive circumferential residual stress computed at the inner diameter of arteries are typically a small fraction of tensile stresses from blood pressure [44, 45] and seemingly of little counteracting benefit. However, using circumferential residual strain as an input for computation of stresses from blood pressure reduces stresses significantly at the inner diameter, as seen by representative results in Fig. 4. Referring to the stress–strain curve in Fig. 5, compressive residual strain will shift the strains from blood pressure to the left, with the shape of the non-linear curve causing stresses from

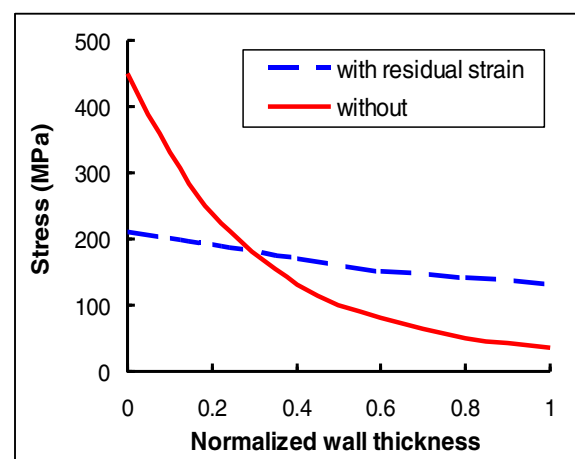


Fig. 4 Effect of residual strains on stresses computed from blood pressure based on data from [46]

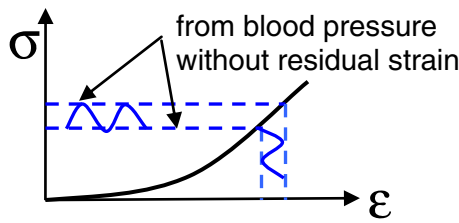


Fig. 5 Schematic of a stress–strain curve for arterial tissue

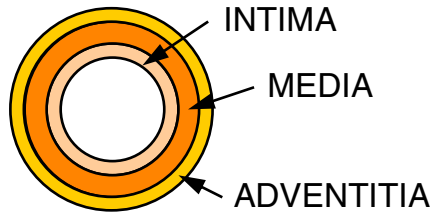


Fig. 6 Cross-section of artery

blood pressures to be much lower than would be predicted by superposition of stresses from blood pressure and residual stresses, each computed separately. This represents a notable difference in residual stress evaluation between biological and engineering materials. Biological materials also typically exhibit anisotropic behavior and varying degrees of viscoelasticity, complicating RSS analysis. The analysis is further complicated for arteries by the presence of three layers, as depicted in Fig. 6, each with its own set of material properties. Details concerning the computation of RSS in arteries based on opening angle data can be found, for example, in Refs. [47–54]. Shortcomings of the opening angle method are discussed in Refs. [13, 29, 54, 55].

The opening angle method has also been used to provide input to computational models [56–59] that attempt to determine the influence of RSS at critical locations in arteries containing atherosclerotic plaque, such as shown by the arrow in Fig. 7(a). The critical location is a region of a fibrous cap overlaying the plaque and vulnerable to rupture. Compressive residual strain reduced stresses from blood pressure at the cap location from 223 to 52 kPa as seen in Fig. 7(c). Validity of the opening angle method in determinations of RSS for the

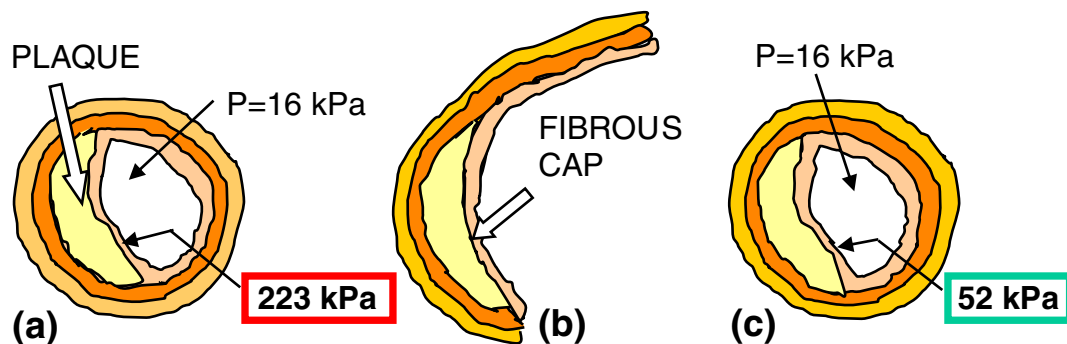


Fig. 7 (a) stresses from blood pressure (16 kPa), (b) opened ring to estimate residual strains, and (c) stresses with influence of RSS based on data in [58]

Fig. 8 Thin-walled tube with a strip cut to determine longitudinal residual stresses

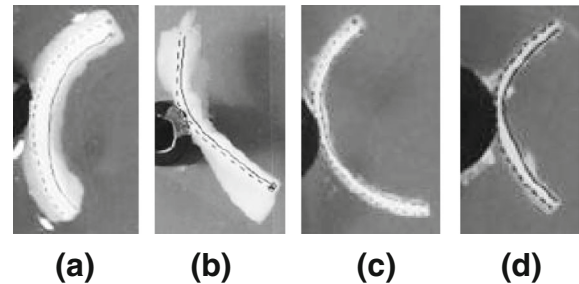
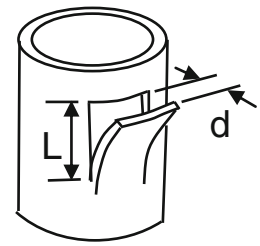


Fig. 9 (a) Longitudinal strip cut from artery, then separated into (b) adventitia, (c) media, (d) intima [78]

complex geometries of arteries with plaque is unknown. The opening angle method has also been applied to study RSS in veins [60], the esophagus [61–64], intestine [65, 66], ventricle of the heart [26, 67–69], tissue-engineered heart chambers [70], trachea [71], airways in lungs [72], brain [73], and an intervertebral (spinal) disc [74]. The method has been a mainstay of studies since the 1980s.

Strip Curling Method

To estimate longitudinal residual stresses in thin-walled tubing, a tongue can be dissected as illustrated in Fig. 8 and the resulting deflection measured, from which residual stresses are computed from the bending moment needed to restore the strip to its original position [75]. A similar approach has been used for arteries, except that the strip is completely separated from an artery [76, 77]. For example, as shown in Fig. 9(a), a strip curls upon removal from an artery and change in length and curvature can be determined approximately. Similar data

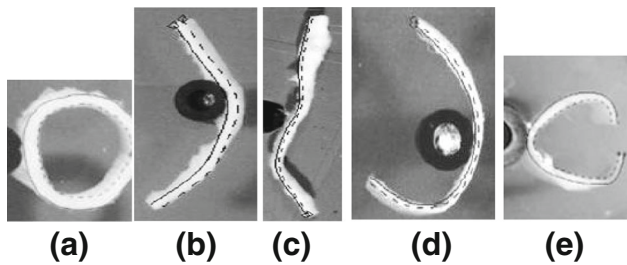


Fig. 10 (a) Ring cut from artery, (b) slit ring, separated into (c) adventitia, (d) media, and (e) intima [78]

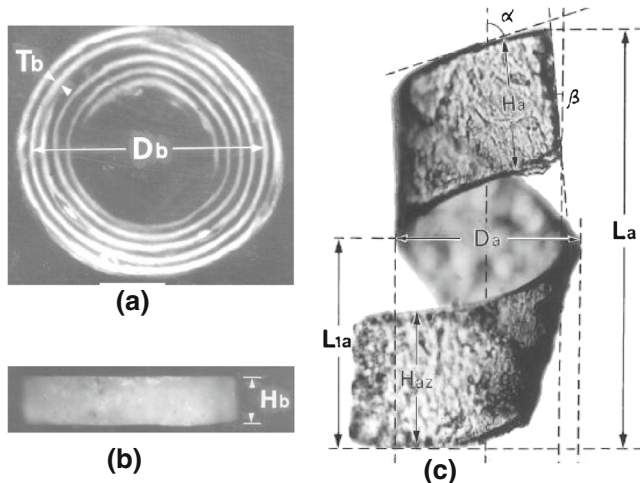


Fig. 11 (a) Cross section of an alternate osteon showing multiple circularly fibered lamellae, (b) ring cut from osteon, (c) shape of an individual lamella after release of residual stresses. Thickness $T_b=5 \mu\text{m}$, diameter $D_b=137 \mu\text{m}$, $H_b=101 \mu\text{m}$ [85]

can be collected for each of the three layers seen in Fig. 9(b)–(d), which were surgically separated from the initial strip. Likewise, opening angle data can be collected for a ring such as that in Fig. 10(a), slit radially as in Fig. 10(b), then separated into the three layers as in Fig. 10(c)–(e). The information obtained from multiple slitting has been used to develop a model to determine the three dimensional state of residual stress in each of three layers [79].

The strip curling method has also been applied to find RSS in intestines [66], stomach [80], cartilage [81, 82], skin [83] and shot peened specimens of bone [84].

As a final example in this section, RSS in cylindrical microstructures in bone known as osteons [22] have been found by a method that might be considered a three dimensional version of opening and curling. Figure 11(a) shows a cross section of a secondary osteon removed from bone. It contains a number of tubular structures, the circularly fibered lamellae. A ring containing the lamellae shown in Fig. 11(b) is obtained by two closely spaced transverse cuts. A single lamella is removed and slit longitudinally, causing it to deflect into the helicoidal shape in Fig. 11(c). An analytical model [85] has been developed to determine both normal and shear residual stresses from measurements of the dimensions and angles of that shape. It is believed [85] that compressive residual stresses in the longitudinal direction and residual shear stresses in the circumferential-longitudinal direction help to protect lamellae from cracking.

Hole Drilling and Ring Coring

A widely applied method for determining residual stresses in engineering materials is based on measurement of strains accompanying the localized release of stresses via introduction of a hole [86, 87]. A related method is ring coring [87], in which residual stresses are released by making a circular trench. Resulting strains measured in the region inside the trench are then related to the residual stresses by finite element modeling.

In the early 1970s, Wright et al. [88] performed a pioneering study in which hole drilling was applied to explore residual stresses in bone. Commercially available strain gage rosettes for holes of 1.6 mm diameter were used. Holes were drilled in one step to a depth equaling the diameter. Transversely isotropic material behavior was assumed for bone and expressions derived relating measured radial strains to residual stresses. Details of the derivation were not presented owing to length

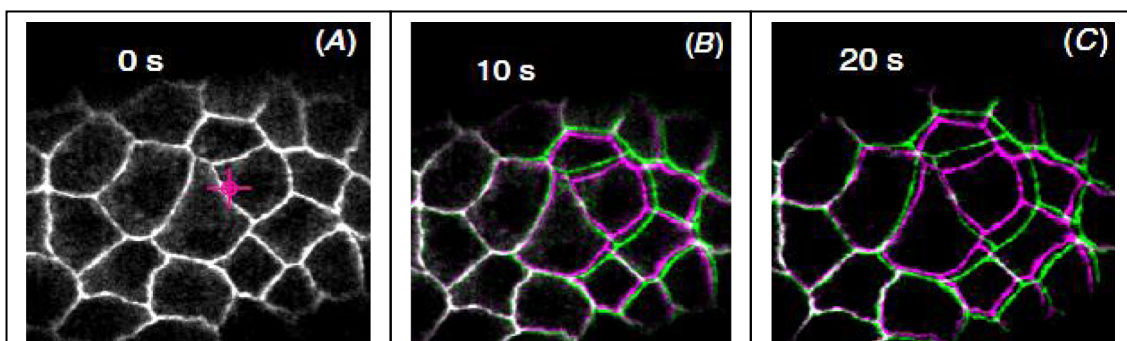


Fig. 12 (a) Image before ablation occurred at cross-hair, (b) overlaid images of cell borders before (magenta) and 10 s after ablation (green) and (c) 20 s after ablation [90] (Reproduced by permission of IOP Publishing)

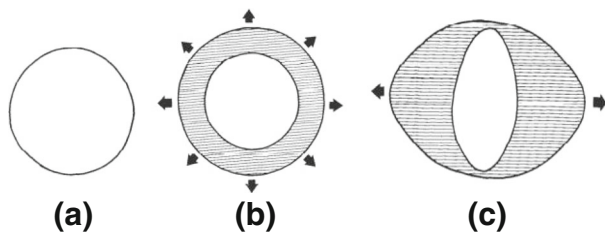


Fig. 13 (a) circle marked on skin, (b) change in wound margin and island for equibiaxial tension, (c) changes in shape for tension varying in direction [92]

limitations on their conference paper. Low levels of residual stresses (1 to 16 MPa) were found in bovine femora, tibia and a radius.

In another version of the hole drilling approach, Varner and Taber [89] perforated epithelia (thin cell sheets) with a specially formed tip of a micropipette, producing holes of about 200 μm diameter. Observed changes in the shapes of the initially circular holes were used with finite element modeling to evaluate stresses in the epithelia. Ma et al. [90] used a laser pulse to ablate a tiny hole (less than 1 μm in diameter) through a layer of cells about 6 μm thick. As illustrated in Fig. 12, sudden introduction of a hole caused recoil of adjacent cells. Image processing was used to capture the displacements during recoil. A model [91] was developed to study the morphogenic stresses associated with the recoil behavior.

In the mid-1800s, Langer [92] used a method similar to ring coring to explore residual stresses in skin by incising around 30 mm diameter circles marked at different locations on cadavers. At locations with equibiaxial tension, the outer

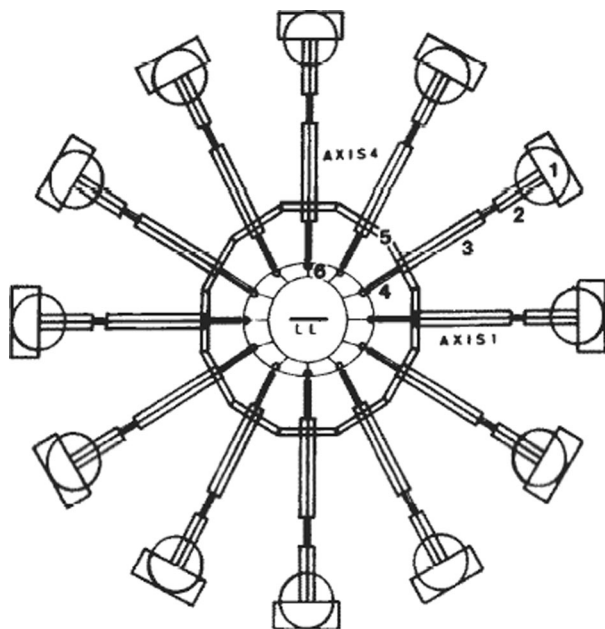


Fig. 14 Schematic of a device used to apply displacements in different directions to a skin specimen shown in the center of the device [93]. Corresponding forces were also measured by the device

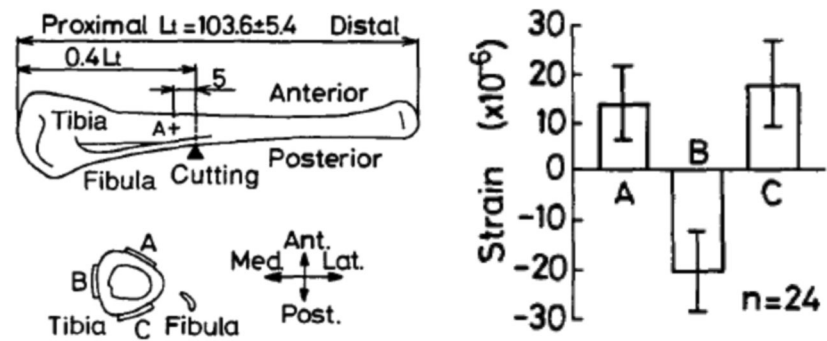
wound margins of circles (Fig. 13(a)) would open, while the central island would shrink, as in Fig. 13(b). At locations where skin tension varied in direction, elliptical shapes like that in Fig. 13(c) were observed. In a 1995 study, 30 mm diameter samples of skin were removed with a circular punch [93]. The resulting samples assumed elliptical shapes. Using a testing device illustrated in Fig. 14, displacements needed to restore the elliptical shape to circular were applied in different directions and corresponding forces measured, from which skin stresses were computed. However, a study [94] in 2008 using circular punches with diameters from 3 to 8 mm revealed what appears to be skin compression. Skin collagen fibers are arranged in a lattice-like pattern of intersecting diamonds. Wounds smaller than the unit size of the lattice may have shrunk as a result of skin structural fibers not having been severed [94], suggesting a sensitivity of the residual stress determination to the volume sampled.

Strains from Dissection

By severing material from its surroundings in an object containing residual stress and measuring resulting strains either in the material severed or in its surroundings, information on RSS can be obtained [95]. Tanaka and Adachi [96] conducted an experiment in which strain gages were applied in the longitudinal direction of a rabbit tibia at locations A, B and C shown in Fig. 15. Severing the fibula induced a change in strains from partial release of residual stresses in the statically indeterminate structure of the tibia and fibula. The authors suggested that the measured strains indicated release of compressive residual stresses on the lateral side of the tibia and tensile stresses on the medial side, but residual stresses were not computed from the strains. In an experiment by Adachi et al. [97], biaxial strain gages were applied to locations L and R in Fig. 16(a) of a bovine vertebra. Strain changes were measured first as the end and growth plates in Fig. 16(a) were removed with a hand saw, then as regions 1 and 2 in Fig. 16(b) were removed successively with a rotary cutter. A simplified analytical model was used to estimate residual stresses. In both longitudinal and circumferential directions, compressive residual stresses were predicted in the cortical region and tensile residual stresses in the cancellous region. Interesting quantitative results may be produced by repeating similar experiments using modern computational tools like finite element modeling.

In another version of dissection, residual strains in the wall of a ventricle of a canine heart have been measured by implanting radio-opaque markers and then removing a block containing the markers and observing changes in position of the markers [98]. In both circumferential and longitudinal directions, tensile residual strains were found in an external layer (epicardium) and compressive strains in the inner layer

Fig. 15 Strains measured by gages at A, B and C upon cutting of fibula [96]



(subendocardium). Torsional shear strains were also found. Residual strains in leaflets (thin flap-like structures) of heart valves have also been measured. Two layers in an aortic valve leaflet, the fibrosa and ventricularis, were separated by microdissection [99], resulting in biaxial elongations of the fibrosa and biaxial contractions of the ventricularis. Upon severing from surrounding tissue, a leaflet from a mitral valve contracted significantly, indicating sizeable residual strains [100]. Residual stresses were not reported in these heart related studies.

Slitting (Crack Compliance)

The slitting (crack compliance) method [101–103] determines the profile of residual stresses vs. depth in engineering materials from strains measured adjacent to a slit as it is gradually deepened. An early form of this approach was applied to bone by Stanwyck et al. [104] in the 1980s. A strain gage was applied in the longitudinal direction to a bovine metatarsal bone and a saw cut was made perpendicular to that axis, 1 mm from the gage and 2 mm deep. The gage registered $-180 \mu\epsilon$. The strain increased to $-280 \mu\epsilon$ when the cut was deepened to 3 mm. No residual stress analysis was reported, which is not

surprising since the slitting method was in its infancy in that era. To measure skin stress, a strain-gage device was developed in the 1980s [105] to measure the forces that developed as skin stress was released by an incision made during surgery. The slitting method has also been applied with finite element modeling [106] to determine tensile residual strains in the periosteum, a thin layer of soft tissue surrounding the outer surface of bones, and in the dura mater [107], a layer of tissue surrounding the brain.

Contour Method

When a flat cross-sectional cut is made to release residual stresses, the resulting contour of the deformed surface can be used to determine the stresses released [108]. By forcing the contour back to its original flat plane by finite element modeling, the residual stresses that existed normal to the plane can be recovered. In perhaps the first application of a version of the contour method to biological material, Matsumoto et al. [109] found that excision of tubular specimens from aortic arteries caused surfaces at the cuts to develop microscopic hills and valleys such as those as seen in Fig. 17. A scanning micro indentation tester was developed to measure stiffness at

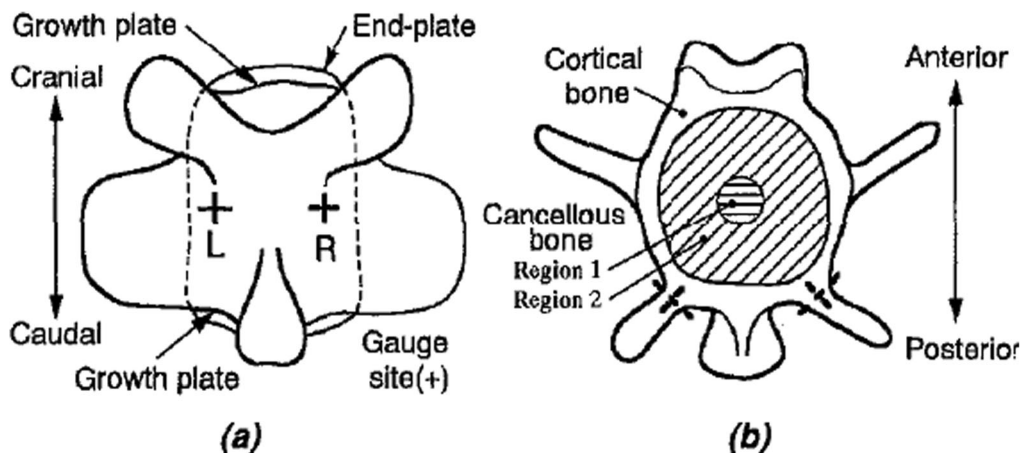
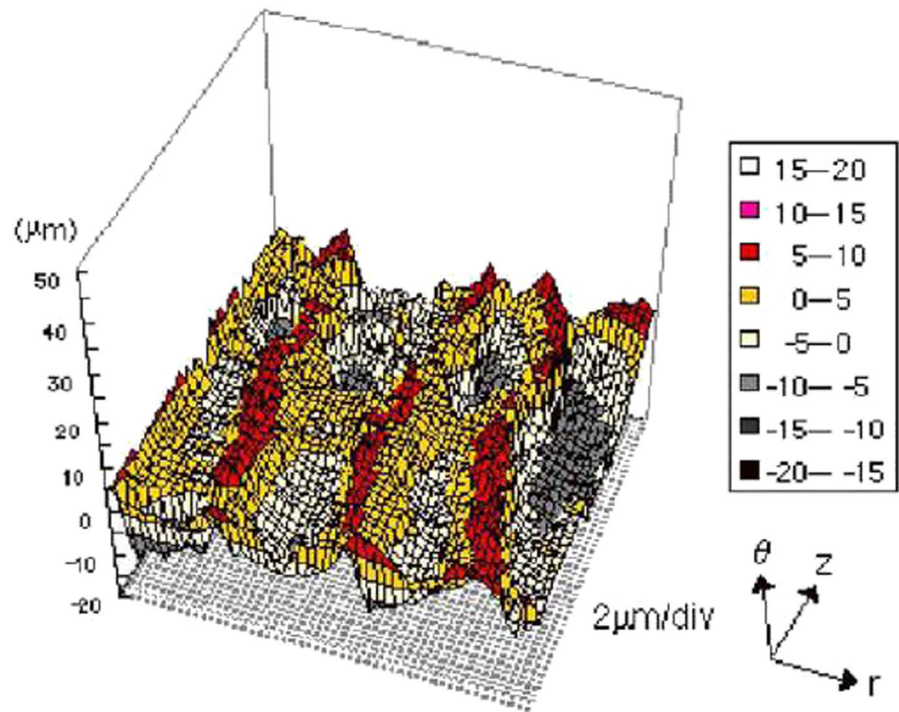


Fig. 16 (a) Posterior and (b) cranial views of bovine vertebra [97]

Fig. 17 Surface topography of a $100 \times 100 \mu\text{m}$ section perpendicular to the circumferential direction of a porcine thoracic aorta [109]



$2 \mu\text{m}$ intervals across the surface. The stiffness in hills was more than triple that in valleys. Residual stresses were estimated as the stresses needed to restore the surface to a flat configuration and were obtained from a finite element model plus measurements of the topography and distribution of stiffness. In another application of the contour method, Badel et al. [110] removed an approximately square sample of tissue from the wall an artery and measured resulting deformations of the six faces using digital image correlation. Specimen faces were on the order of millimeters in size. Residual stresses were reconstructed by finite element modeling.

X-ray Diffraction

The measurement of residual stresses by X-ray diffraction (XRD) is well-established for engineering materials with crystalline structures [111, 112]. Bone contains crystals of hydroxyapatite, enabling XRD to be applied. In 2000, Todoh et al. [113] reported surface residual stresses from an XRD study of specimens cut from a bovine femur and stored in a saline solution prior to testing. Tensile longitudinal stresses between approximately 15 and 40 MPa were found except at the medial location shown in Fig. 18(a), where a compressive stress of -15 MPa was obtained. Circumferential stresses varied from $+5$ to -25 MPa , depending on location. Tadano and Okoshi [114] measured surface longitudinal residual stresses in specimens of rabbit tibiofibula, starting with intact bone and cutting into progressively smaller specimens. The stresses were compressive at some locations shown in

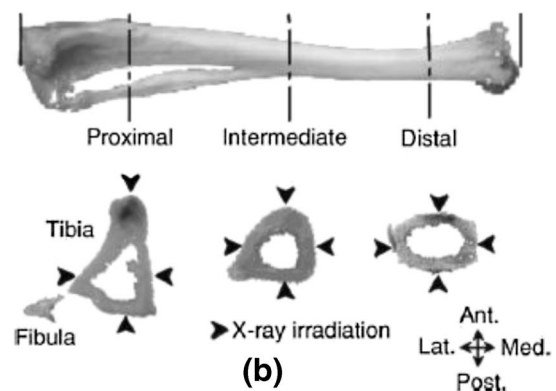
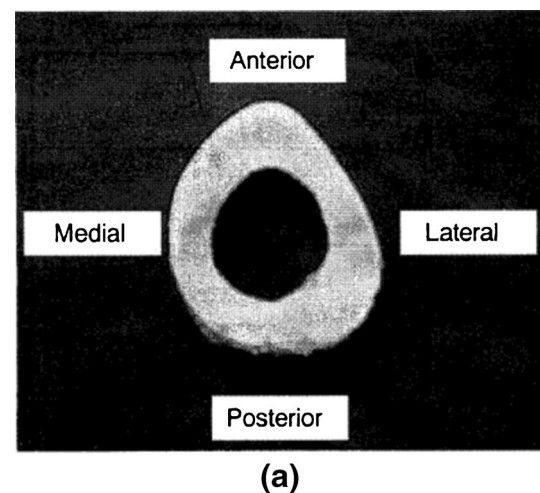


Fig. 18 (a) Locations of specimens taken from a bovine femur [113], (b) measurement locations on a rabbit tibiofibula [114] (Reproduced by permission from IOS Press)

Fig. 18(b), and tensile at others, but relatively small (less than 8 MPa in magnitude) and varied relatively little as a function of cutting sequence. (Circumferential residual stresses were not found because a specimen suitable for XRD calibration could not be obtained in that direction in this study.) Yamada and Tadano [115] found tensile residual stresses (up to 162 MPa) in air-dried specimens cut from bovine femurs. Circumferential residual stresses were smaller than longitudinal stresses (approx. -20 to $+50$ MPa, depending on location). The authors were aware that air drying may have influenced their data. Using synchrotron X-rays [116], Yamada et al. [117] measured longitudinal residual stresses in an air-dried specimen cut from a bovine femur. Measurements were made at the locations depicted in Fig. 19(a), resulting in the variation with depth shown in Fig. 19(b).

Using synchrotron X-rays, Almer and Stock [118] found compressive residual stress in the longitudinal direction of a specimen cut from a canine fibula. They expressed a concern that the stresses may have been associated with dehydration of the specimen. In a subsequent study [119], they found that when a specimen was transferred from storage in formalin (for over 10 months) to a saline solution and kept there for 8 h,

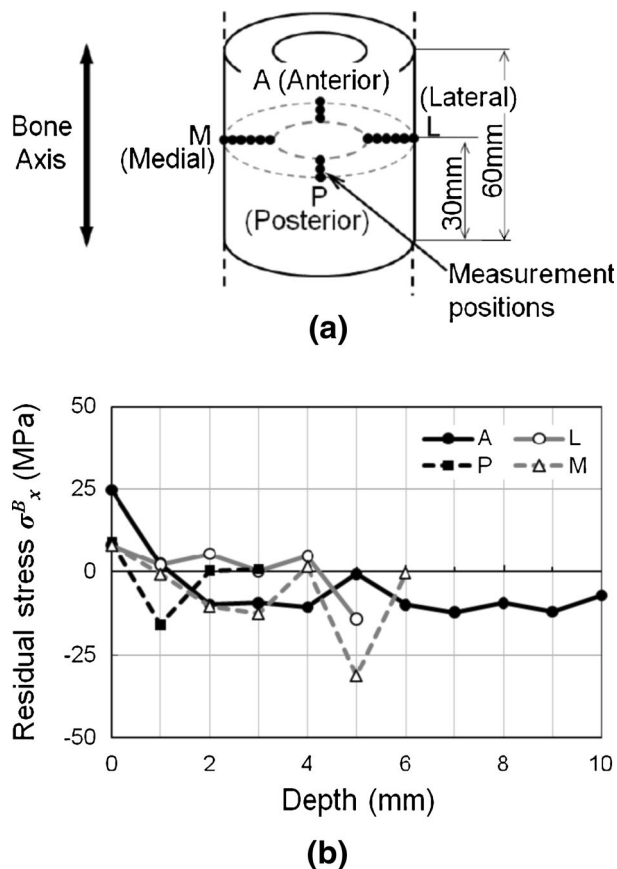


Fig. 19 (a) Measurement locations in specimen taken from bovine femur, (b) longitudinal residual stresses vs. radial position at different locations [117]

residual stresses gradually dropped from about -75 MPa to -10 MPa.

Photoelasticity

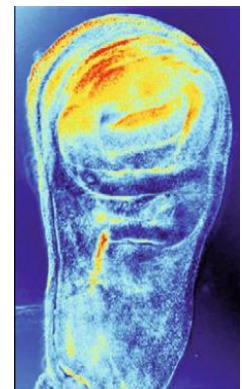
The use of photoelasticity to measure residual stresses in glass and transparent plastics is well established [120]. Aegeter and co-workers [121, 122] have applied principles of photoelasticity and measured the retardance through the thickness of wing imaginal discs of fruit flies. (The discs are structures in the larvae of certain insects that develop into wings in adults.). The distribution of retardance in a typical specimen is shown in Fig. 20. A small loading set-up was used to find the equivalent of stress-optic constants for the disc material. Care was taken to account for changes in retardance from sources other than stress, such as variations in thickness or density of birefringent molecules. Knowledge of how built-in stresses change during morphogenesis is of interest in developmental biology [121].

Membrane and Shell Displacement Methods

Residual stresses in thin membranes of engineering materials can be inferred from their force-displacement behavior, since displacements from application of a force normal to a membrane are a function of residual stress, membrane dimensions, elastic modulus and Poisson's ratio [123, 124]. This type of approach has been extended to the challenging experimental and computational environment of biological materials.

In the 1970s, Alexander & Cook [125] used a device with two cantilevered legs attached to the skin with adhesive pads to measure skin tension forces. A strain gage on one of the legs served as a force sensor. When the legs were brought together, the skin would eventually start to wrinkle (buckle) between the legs, which was taken as indication that zero skin tension had been reached. The corresponding force registered by the device was recorded. Measurements were taken in different directions to produce a polar plot of skin tension at a given location.

Fig. 20 Distribution of retardance in an insect imaginal disc, with red indicating 10 nm retardance [122] (Reproduced by permission from the European Physical Journal)



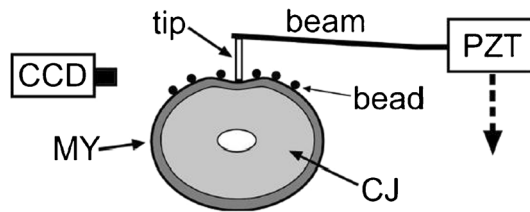


Fig. 21 Cross-section of microindentation test set-up showing myocardium layer (MY), cardiac jelly (CJ), piezoelectric transducer (PZT) and charge-coupled device (CCD) [127]

Diridollou et al. [126] used a suction device to obtain upward displacement vs. pressure data for skin. The data were fitted to an analytical relation for a pre-stressed elastic membrane, derived as a function of pressure, displacement, skin thickness, skin tension and modulus of elasticity. Skin thickness was measured from ultrasound scans. Both skin tension and modulus of elasticity were inferred from data fitting.

At a much smaller size scale, the micro-indentation set-up depicted in Fig. 21 was developed by Zamir and Taber [127, 128] to gather force-displacement and surface contour data for a two cell thick myocardium layer enveloping cardiac jelly, modeled as a thin membrane on an elastic foundation. (Cardiac jelly is a gelatinous substance present during morphogenesis of a heart.) Microspheres (beads) of 6 μm diameter were used to monitor surface displacements. Residual stresses in the myocardium layer were estimated from the force-displacement and surface contour data and an inverse finite element method.

At an even smaller size scale, the force-indentation displacement characteristics of a prohead (an immature viral shell empty of DNA) have been studied by Carrasco et al. [129] with an atomic force microscope. As seen in Fig. 22(a), the prohead had a cylindrical body (radius and length of 20 and 52 nm, respectively) with spherical end caps (radii of 21 nm). The prohead was tested in two orientations shown in Fig. 22(b) using an indenter with a parabolically shaped tip. Finite element modeling indicated the highest indentation stiffness for the upright orientation, while measurements showed the highest stiffness in the horizontal orientation.

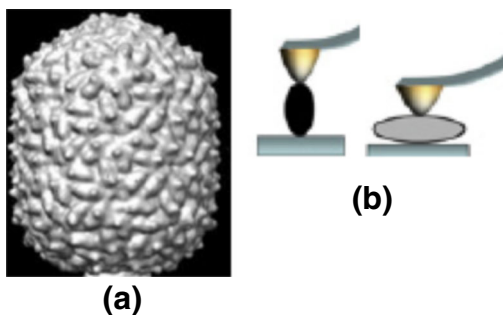
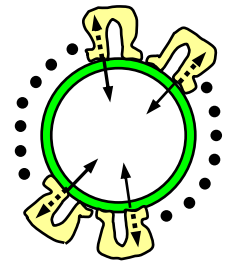


Fig. 22 (a) Prohead, (b) indentation orientations [129]

Fig. 23 Illustration of forces exerted on a virus shell by protrusions based on a model in [130]



Additional modeling suggested that the presence of a tensile lateral residual stress about 1.5 times larger in the cylindrical body than in the end caps could account for observed stiffness behavior. From experimental observations, Baclayon et al. [130] suggested one mechanism creating residual stresses. Protuding features with an arch-like structure shown in Fig. 23 pull a viral shell outwards (dashed arrows) and increase its diameter relative to a shell without the features. The shell, in turn, pulls protruding features inwards (solid arrows).

Certain viral shells of icosahedral form, as in Fig. 24, can develop residual stresses during self-assembly from strain incompatibilities introduced at vertices by mismatches in geometry of different protein sub-units [131]. Force vs. nano-indentation depth experiments were performed on intact viral shells and ones where sources of strain incompatibility were removed, producing a “whiffle ball” structure [131]. The presence of residual stresses was inferred from significant differences in stiffness behavior in the indentation experiments that went beyond those from differences in geometry of intact and whiffle ball shells. Residual stresses in viral shells may serve a protective function [130] but that is a matter of conjecture.

For thoroughness, it should also be noted that cells also contain prestresses (a form of residual stresses) in a cytoskeleton, which is a network of filaments, microtubules, etc. that play an important role in cellular mechanics. Experimental methods for inferring prestresses in cells have been developed in recent years, and a review of methods can be found, for example, in Refs. [132, 133].

Fig. 24 Icosahedron (12 vertices, 20 faces)



Discussion

The studies summarized here provide a sense for the challenges involved in studying RSS in biological structures. For example, the material behavior is often anisotropic, non-linear elastic, viscoelastic and may vary from layer-to-layer in arteries, heart valves, skin, etc. (Details of computing RSS are beyond the scope of this overview, but can be found in the references cited throughout the paper.) Geometries are typically more complicated than for many engineering components. Another complication is that RSS may change as a result of material no longer being alive, and the preparation and handling of specimens may influence results. For example, as shown earlier, residual stresses measured for hydrated [118] and dried [115] specimens of bone can be quite different. Concern over the effect of hydration prompted one research group [104] to attach a strain gage to the hind tibia bone of a live but anesthetized sheep, with wires exiting from within the back of the sheep. A month was allowed to pass for wound healing and natural hydration in the gage area before the area was surgically exposed again, and stress relief measurements made while the area was wetted with saline solution.

An important factor in determining RSS in tissues with muscle cells is the role of muscle contraction. Consider arteries, which contain muscle cells. Opening angles have typically been measured using specimens with relaxed muscle. *In vivo*, muscle in arteries is contracted to a certain extent, which influences stresses in artery walls in ways missed by use of opening angle data obtained with relaxed muscle [134, 135]. Effects of contraction on RSS have been studied with lab specimens. The opening angle increased in rings of rat aortas exposed to the drug norepinephrine, which causes contraction [134]. A similar but smaller effect was observed in nearly all tests of mesenteric, ileocecolic and ileal arteries of rats [136]. Exposure to nitroprusside, which relaxes muscle, reduced the opening angle of rings previously exposed to norepinephrine [134]. On the other hand, saphenous arteries of rats, relaxed with adenosine for 20 min prior to excision from rats, had larger opening angles than control arteries [137]. Effects of muscle contraction on stresses in arterial walls have been explored computationally [135, 138]. Muscle contraction is predicted to increase opening angles, but use of opening angle data from rings with contraction induced by drugs does not appear sufficient to capture the effects of contraction on arterial stresses *in vivo* [135].

Limitations on applicability of the methods reviewed in this article are important to consider but difficult to generalize at present for biological materials. For example, the opening angle method has been widely applied to arteries and other soft tissue structures, where deflections upon release of RSS are sizeable. Suppose that the same method was applied to a ring of bone such as that shown in Fig. 18(a) in an attempt to determine circumferential residual stresses. It would probably

produce misleading results. A very small deflection would likely occur because of the relatively high stiffness of bone, coupled with residual stresses varying in depth like those in Fig. 19(b) rather than as a bending distribution through the thickness, as with arteries. The deflection, if measurable, might lead to the incorrect conclusion that residual stresses were essentially nonexistent in bone. On the other hand, an incremental slitting version of the opening angle method might give very different results. Measurement of surface strains as a radial slit was deepened, combined with finite element modeling, could be a viable approach. As mentioned previously, slitting to a depth of 2 mm gave strains of $-180 \mu\epsilon$ near the slit from release of longitudinal stresses in a bone specimen [104]. If similar magnitudes of strain occur in the circumferential direction, then an incremental slitting version of the opening angle method, starting at depths closer to the surface than 2 mm, may be feasible for bone. Careful consideration should be given on a case-by-case basis before a method is applied, taking into account factors such as the ability to measure deflections, displacements or strains with sufficient precision and the ability of a computational model for determining RSS to incorporate the complexities of the material behavior being investigated.

The volume of biological material sampled by an experimental method can also have a marked effect on determination of RSS. For instance, residual stresses determined in bone by hole drilling using standard-sized strain gage rosettes [88] were quite different than those determined by relieving stresses in a small structural unit such as a lamella in an osteon [85]. A similar “size effect” was seen in experiments in which different diameter circles were incised in skin [92–94]. Such effects are reminiscent of differences in residual stresses in engineering materials with different measurement volumes. In metals, for example, micro-residual stresses in individual grains may be quite different than macro-residual stresses measured over larger volumes [139].

Opportunities may exist to further adapt existing approaches for determining RSS in biological structures. In studies of skin, for example, determinations of RSS by excision around a circle do not appear to have accounted for differences in stress–strain behavior of different layers of skin (e.g., epidermis, dermis, etc.). It may be possible to find RSS on a layer-by-layer basis by a technique similar to incremental ring coring, together with finite element modeling and optical measurement of surface displacements. The slitting and contour methods have been applied in relatively few studies of biological RSS so far. It may be possible, for example, to apply the contour method to cross-sectional areas of bone with a suitable means of cutting and finite element modeling that accounts for differences in elastic constant of microstructural units such as osteons and interstitial lamellae. It may also be possible to re-evaluate experimental data from earlier RSS studies using computational capabilities that did not exist when the studies were done.

The future seems likely to see development of new experimental approaches for determining RSS in the size regime of cells and smaller. Approaches may be devised that utilize new sensor technologies. For example, a sensor has been developed that can be inserted into structural proteins to measure molecular strains [140]. It consists of two proteins that fluoresce when exposed to light, linked by an elastic, coiled protein structure. Strains cause measureable changes in fluorescence energy characteristics.

Summary

Residual stresses and strains exist in biological structures ranging from blood vessels to virus shells are believed to have important physiological functions, and generally need to be taken into account in computational models of biomechanical behavior.

Most experimental methods for determining residual stresses and strains in biological structures parallel those developed for engineering components, but adapted to the experimental challenges presented by biological materials and the computational complexities of non-linear, anisotropic and often viscoelastic material behavior.

Opportunities may exist to advance the determination of residual stresses and strains in biological structures through adaptation of approaches such as hole drilling, slitting, the contour method and others, taking advantage of experimental techniques (e.g., digital image correlation) and computational modeling capabilities developed in recent years in the field of experimental mechanics.

References

1. Taber L (1995) Biomechanics of growth, remodeling and morphogenesis. *Appl Mech Rev* 48(8):487–545
2. Taber L (2001) Biomechanics of cardiovascular development. *Annu Rev Biomed Eng* 3:1–2
3. Rodriguez E, Hoger A, McCulloch A (1994) Stress-dependent finite growth in soft elastic tissues. *J Biomech* 27:455–467
4. Skalak R, Zargaryan S, Jain R, Netti P, Hoger A (1996) Compatibility and the genesis of residual stress by volumetric growth. *J Math Biol* 34:889–914
5. Vandiver R, Goriely A (2009) Differential growth and residual stress in cylindrical elastic structures. *Phil Trans R Soc A* 367:3607–3630
6. Olsson T, Klarbring A (2008) Residual stresses in soft tissue as a consequence of growth and remodeling: an application to an arterial geometry. *Eur J Mech A-Solid* 27:959–974
7. Wells S, Walter E (2010) Changes in the mechanical properties and residual strain of elastic tissue in the developing fetal aorta. *Ann Biomed Eng* 38:345–356
8. Ambrosi D, Guillou A, DiMartino E (2008) Stress-modulated remodeling of a non-homogeneous body. *Biomech Model Mechanobiol* 7:63–76
9. Yeni Y, Schaffler M, Gibson G, Fyhrie D (2002) Prestress due to dimensional changes caused by demineralization: a potential mechanism for microcracking in bone. *Ann Biomed Eng* 30:217–225
10. Volokh K, Lev Y (2005) Growth, anisotropy and residual stresses in arteries. *Mech Chem Biosyst* 2:27–40
11. Karsaj I, Humphrey J (2012) A multilayered wall model of arterial growth and remodeling. *Mech Mater* 44:110–119
12. Rachev A (1997) Theoretical study of the effect of stress-dependent remodeling on arterial geometry under hypertensive conditions. *J Biomech* 30:819–827
13. Taber L, Humphrey J (2001) Stress-modulated growth, residual stress and heterogeneity. *J Biomech Eng* 123:528–535
14. Archer R (1987) Growth stresses and strains in trees. Springer, Berlin
15. Cardamone L, Valentin A, Eberth J, Humphrey J (2009) Origin of axial prestretch and residual stress in arteries. *Biomech Model Mechanobiol* 8:431–446
16. Araujo R, McElwain D (2005) A mixture theory for the genesis of residual stresses in growing tissues I: a general formulation. *SIAM J Appl Math* 65:1261–1284
17. Ateshian G, Ricken T (2010) Multigenerational interstitial growth of biological tissues. *Biomech Model Mechanobiol* 9:689–702
18. Lanir Y (2012) Osmotic swelling and residual stress in cardiovascular tissues. *J Biomech* 45:780–789
19. Azeloglu E, Albro M, Thimmappa V, Ateshian G, Cosat K (2007) Heterogeneous transmural proteoglycan distribution provides a mechanism for regulating residual stresses in the aorta. *Am J Physiol Heart Circ Physiol* 294:H1197–H1205
20. Cowin S (2004) Tissue growth and remodeling. *Ann Rev Biomed Eng* 6:77–107
21. Carter D, Beaupre G (2001) Skeletal function and form. Cambridge University Press, Cambridge
22. Currey J (2002) Bones. Princeton University Press, Princeton
23. Taber L, Eggers D (1996) Theoretical study of stress-modulated growth in the aorta. *J Theor Biol* 180:343–357
24. Ambrosi D, Ateshian G, Arruda E, Cowin S, Dumais J, Goriely A, Holzapfel G, Humphrey J, Kemkemer R, Kuhl E, Olberding J, Taber L, Garikipati K (2011) Perspectives on biological growth and remodeling. *J Mech Phys Solids* 59:863–883
25. Gonzalez-Torres L, Gomez-Benito M, Garcia-Aznar J (2011) Evaluation of residual stresses due to bone callus growth: a computational study. *J Biomech* 44:1782–1787
26. Taber L, Hu N, Peixeider T, Clark E, Keller B (1993) Residual strain in the ventricle of the stage 16–24 chick embryo. *Circ Res* 72:455–462
27. Henderson CD (2002) Mechanical induction in limb morphogenesis: the role of growth-generated strains and pressures. *Bone* 11:645–653
28. Fung Y (1991) What are the residual stresses doing in our blood vessels? *Ann Biomed Eng* 19:237–249
29. Rachev A, Greenwald S (2003) Residual strains in conduit arteries. *J Biomech* 36:661–670
30. Destrade M, Liu Y, Murphy J, Kassab G (2012) Uniform transmural strain in pre-stresses arteries occurs at physiological pressure. *J Theor Biol* 303:93–97
31. Delfino A, Stergiopoulos N, Moore J, Meister J (1997) Residual strain effects on the stress field in a thick wall finite element model of the human carotid bifurcation. *J Biomech* 30:777–786
32. Volokh K (2008) Prediction of arterial failure based on microstructural bi-layer fiber-matrix model with softening. *J Biomech* 41:447–453
33. Ohayon J, Dubreuil O, Tracqui P, LeFloc'h S, Rioufol G, Chalabreysse L, Thivolet F, Pettigrew R, Finet G (2007) Influence of residual stress/strain on the biomechanical stability of vulnerable coronary plaques: potential impact for evaluating the risk of plaque rupture. *Am J Physiol Heart Circ Physiol* 293:H1987–H1996
34. Wang C, Kassab G (2009) Increase in opening angle in hypertension off-loads the intimal stress: a simulation study. *J Biomech Eng* 131:114502. doi:10.1115/1.4000085

35. Fung Y, Liu S (1991) Change in zero-stress state of rat pulmonary arteries in hypoxic hypertension. *J Appl Physiol* 70:2455–2470
36. Horny L, Adamek T, Zitny R (2013) Age-related changes in longitudinal prestress in human abdominal aorta. *Arch Appl Mech* 83: 875–888
37. Cacho F, Doblare M, Holzapfel G (2007) A procedure to simulate coronary artery bypass graft surgery. *Med Biol Eng Comput* 45:819–827
38. Zhao X, Liu Y, Zhang W, Wang C, Kassab G (2011) A novel arterial constitutive model in a commercial finite element package: application to balloon angioplasty. *J Theor Biol* 286:92–99
39. Gurtner G, Dauskardt R, Wong V, Bhatt K, Wu K, Vial I, Padois K, Korman J, Longacker M (2011) Improving Cutaneous scar formation by controlling the mechanical environment. *Ann Surg* 254:217–225
40. Capek L, Jacquet E, Dzan L, Simunek A (2012) The analysis of forces needed for the suturing of elliptical skin wounds. *Med Biol Eng Comput* 50:193–198
41. ASTM Standard E1928, 2007, Standard practice for estimating the approximate residual circumferential stress in straight thin-walled tubing, ASTM International, West Conshohocken, PA. doi:10.1520/E1928-07
42. Fung Y (1984) *Biodynamics: circulation*. Springer, New York, pp 54–60
43. Vishnav R, Vossoughi, J (1983) Estimation of residual strains in aortic segments. In: Hall C (ed) *Biomedical engineering II, recent developments* pp 330–333
44. Choung C, Fung Y (1986) On residual stresses in arteries. *J Biomech Eng* 108:189–192
45. Raghavan M, Trivedi S, Nagaraj A, McPherson D, Chandran K (2004) Three-dimensional finite element analysis of residual stresses in arteries. *Ann Biomed Eng* 32:257–263
46. Zhang W, Herrera C, Atluri S, Kassab G (2005) The effect of longitudinal pre-stress and radial constraint on the stress distribution in the vessel wall: a new hypothesis. *Mol Cell Biomech* 2: 41–52
47. Humphrey J (2002) *Cardiovascular solid mechanics: cells, tissues and organs*. Springer, New York
48. Holzapfel G, Gasser T, Ogden R (2000) A new constitutive framework for arterial wall mechanics and a comparative study of material models. *J Elast* 61:1–48
49. Alastrue V, Martinez M, Doblare M (2008) Modeling adaptive volumetric finite growth in patient-specific residually stressed arteries. *J Biomech* 41:1773–1781
50. Alford P, Humphrey J, Taber L (2008) Growth and remodeling in a thick-walled artery model: effects of spatial variations in wall constituents. *Biomech Model Mechanobiol* 7:245–262
51. Hollander Y, Durban D, Lu X, Kassab G, Lanir R (2011) Constitutive modeling of coronary arterial media-comparison of three model cases. *J Biomech Eng* 133:061008-1–061008-12
52. Stylianopoulos T, Barocas V (2007) Multiscale, structure-based modeling for the elastic mechanical behavior of arterial walls. *J Biomech Eng* 129:611–618
53. Greenwald S et al (1997) Experimental investigation of the distribution of residual strains in the artery wall. *J Biomech Eng* 119:438–444
54. Van Dyke T, Hoger A (2002) A new method for predicting the opening angle for soft tissues. *J Biomech Eng* 124:347–354
55. Olsson T, Satlhand J, Klarbring A (2006) Modeling initial strain distribution in soft tissues with applications to arteries. *Biomech Model Mechanobiol* 5:27–38
56. Ohanyon et al (2007) Influence of residual stress/strain on the biomechanical stability of vulnerable coronary plaques: potential impact for evaluating the risk of plaque rupture. *Am J Physiol Heart Circ Physiol* 293:H1987–H1996
57. Balzani D, Schroder J, Gross D (2007) Numerical simulation of residual stresses in arterial walls. *Comput Mater Sci* 39:117–123
58. Broisat A et al (2011) Assessing low levels of mechanical stress in aortic atherosclerotic lesions from apolipoprotein E^{-/-} mice – brief report. *Arterioscler Thromb Vasc Biol* 31:1007–1010
59. Cilla M, Pena E, Martinez M (2012) 3D computational parametric analysis of eccentric atheroma plaque: influence of axial and circumferential residual stress. *Biomech Model Mechanobiol* 11:1001–1013
60. Xie J et al (1991) The zero-stress state of rat veins. *J Biomech Eng* 113:36–41
61. Gregersen H, Lee T, Chien S, Skalak R, Fung Y (1999) Strain distribution in the layered wall of the esophagus. *J Biomech Eng* 121:442–448
62. Laio D, Fan Y, Zeng G, Gregersen H (2003) Stress distribution in the layered wall of the rat oesophagus. *Med Eng Phys* 25:731–738
63. Zhao J et al (2007) Opening angle and residual strain in a three-layered model of pig oesophagus. *J Biomech* 40:3187–3192
64. Sokolis D (2010) Strain-energy function and three-dimensional stress distribution in esophageal biomechanics. *J Biomech* 43: 2753–2764
65. Gao C, Gregersen H (2000) Biomechanical and morphological properties in rat large intestine. *J Biomech* 33:1089–1097
66. Dou Y et al (2006) Longitudinal residual strain and stress-strain relationship in rat small intestine. *Biomed Eng Online* 5:37. doi:10.1186/1475-925-5-37
67. Omens J, Fung Y (1990) Residual strain in rat left ventricle. *Circ Res* 66:37–45
68. Summerour S, Emery J, Fazell B, Omesn J, McCulloch A (1998) Residual strain in ischemic ventricular myocardium. *J Biomech Eng* 120:710–714
69. Omens J, McCulloch A, Crisicone J (2003) Complex distribution of residual stress and strain in the mouse left ventricle: experimental and theoretical models. *Biomech Model Mechanobiol* 1:267–277
70. Lee E, Kim D, Azeloglu E, Costa K (2007) Engineered cardiac organoid chambers: toward functional biological model ventricle. *Tissue Eng A* 14:215–225
71. Han H, Fung Y (1991) Residual strains in porcine and canine trachea. *J Biomech* 24:307–315
72. McKay K et al (2002) Zero-stress state of intra- and extraparenchymal airways from human, pig, rabbit and sheep lungs. *J Appl Physiol* 92: 1261–1266
73. Xu G, Bayly P, Taber L (2009) Residual stress in the adult mouse brain. *Biomech Model Mechanobiol* 8:253–262
74. Michalek A, Gardner-Morse M, Iatridis J (2012) Large residual strains are present in the intervertebral disc annulus fibrosus in the unloaded state. *J Biomech* 45:1227–1231
75. Sachs G, Espey G (1942) A new method for determination of stress distribution in thin-walled tube. *Trans Am Inst Min Metall Eng* 147: 348–360
76. Vossoughi J (1992) Longitudinal residual strains in arteries. In: *Digest of papers, Eleventh Southern Biomedical Engineering Conference*, Memphis State University, Memphis, TN, pp. 17–19
77. Wang L, Gleason R (2010) A mechanical analysis of conduit arteries accounting for longitudinal residual strains. *Ann Biomed Eng* 38: 1377–1387
78. Holzapfel G et al (2007) Layer-specific 3D residual deformation of human aortas with non-atherosclerotic intimal thickening. *Ann Biomed Eng* 35:530–545
79. Holzapfel G, Ogden R (2010) Modeling the layer-specific three-dimensional residual stresses in arteries, with an application to the human aorta. *J R Soc Interface* 7:787–799
80. Zhao J, Liao D, Gregersen H (2005) Tension and stress in the rat and rabbit stomach are location- and direction-dependent. *Neurogastroenterol Motil* 17:388–398
81. Setton L, Tohyama H, Mow V (1998) Swelling and curling behaviors of articular cartilage. *J Biomech Eng* 120:355–361

82. Wan L, Guo X, Mow V (2010) A triphasic orthotropic laminate model for cartilage curling behavior: fixed charge density versus mechanical property inhomogeneity. *J Biomech Eng* 132:024504-1–024504-5
83. Matsumoto T, Ikuta N, Mori M, Nagayam K (2010) Mechanics of wrinkle formation: micromechanical analysis of skin deformation during wrinkle formation in ultraviolet-irradiated mice. *Skin Res Technol* 16:179–189
84. Hizal A, Sadasivam B, Arola D (2008) Residual stress in bone: a parametric study. In: Proc. 2008 ASME International Mechanical Engineering Congress and Exposition, paper no. IMECE2008-68944, American Society of Mechanical Engineers, New York
85. Ascenzi M (1999) A first estimation of prestress in so-called circularly fibered osteonic lamellae. *J Biomech* 32:935–942
86. ASTM Standard E837, 2008e2, Standard test method for determining residual stresses by the hole-drilling strain-gage method, ASTM International, West Conshohocken, PA. doi:10.1520/E0837-08E02
87. Schajer G, Whitehead P (2013) Hole drilling and ring coring (chapter 2). In: Schajer G (ed) Practical residual stress measurement methods. Wiley, Chichester, pp 29–64
88. Wright T, Barnett D, Hayes W (1977) Residual stress in bone. In: Chang T (ed) Recent advances in engineering science, vol 8, part III of Proc Tenth Anniversary Meeting of Soc Eng Sci (held in 1973). Scientific Publishers, Boston, pp 25–32
89. Varner V, Taber L (2010) On measuring stress distributions in epithelia. In: Garikipati K, Arruda E (eds) IUTAM symposium on cellular, molecular and tissue mechanics, IUTAM bookseries 16. Springer, New York, pp 45–54
90. Ma X et al (2009) Probing embryonic tissue mechanics with laser hole drilling. *Phys Biol*. doi:10.1088/1478-3975/6/3/036004
91. Hutson M et al (2009) Combining laser microsurgery and finite element modeling to assess cell-level epithelial mechanics. *Biophys J* 97:3075–3085
92. Langer K (1978) On the anatomy and physiology of the skin. II. Skin tension. *Br J Plast Surg* 31:93–106 (translation of an 1862 article)
93. Reishner R, Balogh B, Menzel E (1995) Two-dimensional elastic properties of human skin in terms of an incremental model at the in-vivo configuration. *Med Eng Phys* 17:304–313
94. Bush J, Ferguson M, Mason T, McGrouther D (2008) Skin tension or skin compression? Small circular wounds are likely to shrink, not gape. *J Plast Reconstr Aesthet* 61:529–534
95. Ruud C (2002) Measurement of residual stresses. In: Totten G, Howes M, Inoue T (eds) Handbook of residual stress and deformation in steel. ASM International, Materials Park, pp 99–117
96. Tanaka M, Adachi T (1994) Preliminary study on mechanical bone remodeling permitting residual stress. *JSME Int J A-Mech M* 37:87–95
97. Adachi T, Tanaka M, Tomita Y (1998) Uniform stress state in bone structure with residual stress. *J Biomech Eng* 120:342–347
98. Costa K, May-Newman K, Farr D, O'Dell W, McCulloch A, Omens J (1997) Three-dimensional residual strains in midanterior canine left ventricle. *Am J Physiol (Heart Circ Physiol)* 273: H1968–H1976
99. Stella J, Sacks M (2007) On the biaxial mechanical properties of the layers of the aortic valve leaflet. *J Biomech Eng* 129:757–766
100. Amini R et al (2012) On the in vivo deformation of the mitral valve anterior leaflet: effects of annular geometry and referential configuration. *Ann Biomed Eng* 40:1455–1467
101. Prime M (1999) Residual stress measurement by successive extension of a slot: the crack compliance method. *Appl Mech Rev* 52:75–96
102. Cheng F, Finnie I (2007) Residual stress measurement and the slitting method. Springer, New York
103. Hill M (2013) Slitting. (chapter 4). In: Schajer G (ed) Practical residual stress measurement methods. Wiley, Chichester, pp 89–108
104. Stanwyck T, Fischer R, Pope M, Seligson D (1982) Studies on prestress in bone. *Biorheol* 19:301–306
105. Jones M, Pouchak M, Mikelsons R (1987) A method for measuring skin tension. In: Biomedical sciences instrumentation, vol. 23, Instrument Society of America, Research Triangle Park, NC, pp. 199–205.
106. Chen J, Zhao B, Longaker M, Helms J, Carter D (2008) Periosteal biaxial residual strains correlate with bone specific growth rates in check embryos. *Comput Method Biomech* 11:453–461
107. Henderson J, Nacamuli R, Zhao B, Longaker M, Carter D (2005) Age-dependent residual tensile strains are present in the dura mater of rats. *J R Soc Interface* 2:159–167
108. Prime M, DeWald A (2013) Contour method (chapter 5). In: Schajer G (ed) Practical residual stress measurement methods. Wiley, Chichester, pp 109–138
109. Matsumoto T, Goto T, Furukawa T, Sato M (2004) Residual stress and strain in the lamellar unit of the porcine aorta: experimental analysis. *J Biomech* 37:807–815
110. Badel P, Genovese K, Avril S (2012) 3D residual stress field in arteries: novel inverse method based on optic full-field measurement. *Strain* 48:528–538
111. Noyan I, Cohen J (1987) Residual stress: measurement by diffraction and interpretation. Springer, New York
112. Noyan C, Murray C (2013) X-ray diffraction (chapter 6). In: Schajer G (ed) Practical residual stress measurement methods. Wiley, Chichester, pp 139–161
113. Todoh M, Tadano S, Shibano J, Ukai T (2000) Polychromatic X-ray measurements of anisotropic residual stress in bone femoral bone. *JSME Int J C - Mech Syst* 43:795–801
114. Tadano S, Okoshi T (2006) Residual stress in bone structure and tissue of rabbit's tibiofibula. *Bio-Med Mater Eng* 16:11–21
115. Yamada S, Tadano S (2010) Residual stress around the cortical surface in bovine femoral diaphysis. *J Biomech Eng* 132:044503-1–044503-4
116. Withers P (2013) Synchrotron diffraction (chapter 7). In: Schajer G (ed) Practical residual stress measurement methods. Wiley, Chichester, pp 163–184
117. Yamada S, Tadano S, Todoh M, Fujisaki K (2011) Residual stress distribution in the bovine femoral diaphysis measured by synchrotron. *J Biomech Sci Eng* 6:114–124
118. Almer J, Stock S (2005) Internal strains and stresses measured in cortical bone via high-energy X-ray diffraction. *J Struct Biol* 152: 14–27
119. Almer J, Stock S (2007) Micromechanical response of mineral and collagen phases in bone. *J Struct Biol* 157:365–370
120. ASTM Standard D 4093-95 (2010) Standard test method for photoelastic measurements of birefringence and residual strains in transparent or translucent plastic materials, ASTM International, West Conshohocken, PA. doi:10.1520/D4093-95R10
121. Nienhaus U, Aegeer-Wilmsen T, Aegeer C (2009) Determination of mechanical stress distribution in Drosophila wing discs using photoelasticity. *Mech Dev* 126:942–949
122. Schluck T, Aegeer C (2010) Photo-elastic properties of the wing imaginal disc of drosophila. *Eur Phys J E33*:111–115
123. Crowe K, Smith R (1989) A new technique for determination of tensile stress in thin films. *J Electrochem Soc* 136:1566–1568
124. Hong T et al (1990) Measuring stiffnesses and residual stresses of silicon nitride thin films. *J Electron Mater* 19:903–909
125. Alexander H, Cook T (1977) Accounting for natural tension in the mechanical testing of human skin. *J Invest Dermatol* 69:310–314
126. Dirdollou S et al (2000) Sex- and site-dependent variations in the thickness and mechanical properties of human skin in vivo. *Int J Cosmet Sci* 22:421–435
127. Zamir E, Taber L (2004) On the effects of residual stress in microindentation tests of soft tissue structures. *J Biomech Eng* 126:276–283

128. Zamir E, Taber L (2004) Material properties and residual stress in the stage 12 chick heart during cardiac looping. *J Biomech Eng* 126:823–830
129. Carrasco C et al (2011) Built-in mechanical stress in viral shells. *Biophys J* 100:1100–1108
130. Baclayon M et al (2011) Prestress strengthens the shell of norwalk virus nanoparticles. *Nano Lett* 11:4865–4869
131. Klug W, Roos W, Wuite G (2012) Unlocking internal prestress from protein nanoshells. *Phys Rev Lett* 109:168104-1–168104-5
132. Stamenovic D (2012) Cytoskeletal prestress as a determinant of deformability and rheology of adherent cells. In: Obradovi B (ed) *Cell and tissue engineering*. Springer, Berlin, pp 92–118
133. Park C, Tambe D, Alencar A, Trepas X, Zhou E, Millet E, Butler J, Fredberg J (2010) Mapping the cytoskeletal prestress. *Am J Physiol* 298:C1245–C1252
134. Matsumoto T, Tsuchida M, Sato M (1996) Change in intramural strain distribution in rat aorta due to smooth muscle contraction and relaxation. *Am J Physiol* 271:H1711–H1716
135. Rachev A, Hayashi K (1999) Theoretical study of the effects of vascular smooth muscle contraction on strain and stress distributions in arteries. *Ann Biomed Eng* 27:459–468
136. Fung Y, Liu S (1992) Strain distribution in small blood vessels with zero-stress state taken into consideration. *Am J Physiol* 262:H544–H552
137. Zeller P, Skalak T (1998) Contributions of individual structural components in determining the zero-stress state in small arteries. *J Vasc Res* 35:8–17
138. Yamada H, Shinoda T, Tanaka E, Yamamoto S (1999) Finite element modeling and numerical simulation of the artery in active state. *JSME Int J C - Mech Syst* 42:501–507
139. Withers P, Bhadeshia H (2001) Residual stress. Part I – measurement techniques. *Mater Sci Technol* 17:355–365
140. Wang Y, Meng F, Sachs F (2011) Genetically encoded force sensors for measuring mechanical forces in proteins. *Commun Integr Biol* 4: 385–390